Lawrence Berkeley Laboratory
UNIVERSITY OF CALIFORNIA

Materials & Molecular Research Division

Presented at the International Conference on Thermal Stresses in Materials and Structures in Severe Thermal Environments, Virginia Polytechnic Institute and State University, Blacksburg, VA, March 19-21, 1980; and published in the proceedings

RESIDUAL STRESSES AND MICROCRACKING INDUCED BY THERMAL CONTRACTION INHOMOGENEITY

A.G. Evans and D.R. Clarke

September 1980

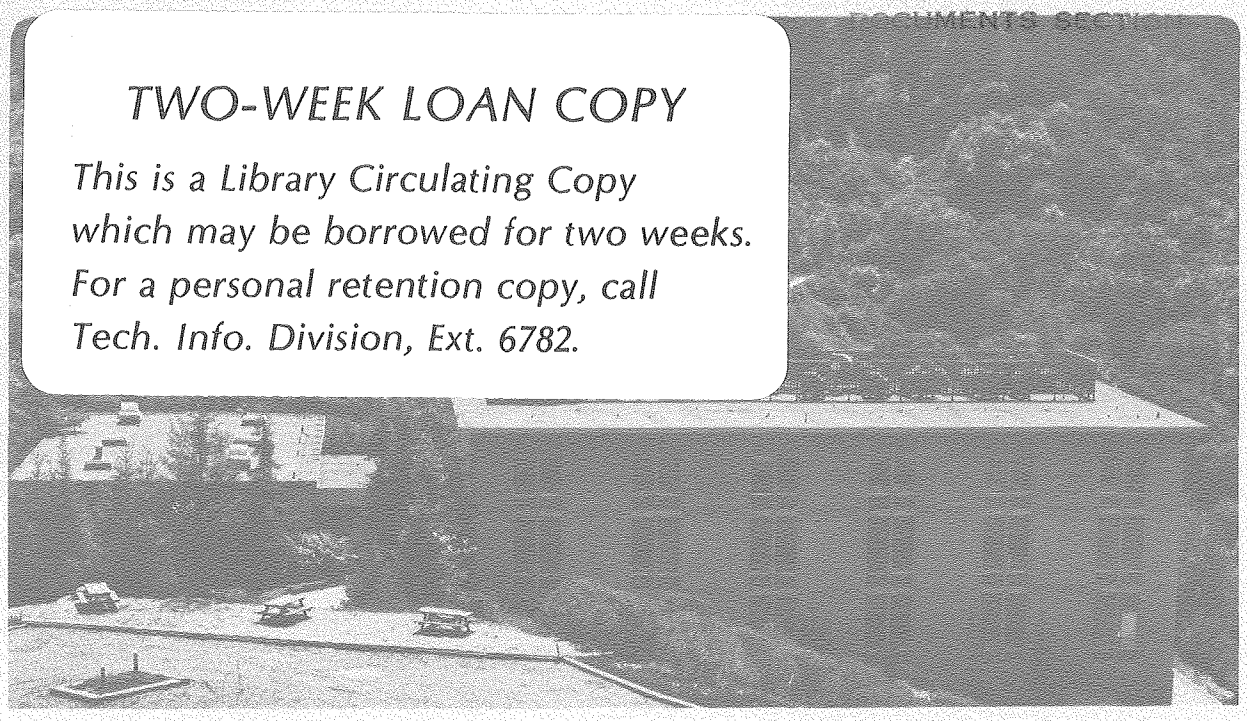

Prepared for the U.S. Department of Energy under Contract W-7405-ENG-48

DISCLAIMER

LBL-11568

RESIDUAL STRESSES AND MICROCRACKING INDUCED BY THERMAL CONTRACTION INHOMOGENEITY

by

A.G. Evans
Department of Materials Science and Mineral Engineering
Lawrence Berkeley Laboratory
University of California
Berkeley, CA 94720

and

D.R. Clarke
Structural Ceramics Group
Rockwell International Science Center
Thousand Oaks, CA 91360

RESIDUAL STRESSES AND MICROCRACKING INDUCED BY THERMAL CONTRACTION INHOMOGENEITY

A.G. Evans* and D. R. Clarke†

University of California, Berkeley* and
Rockwell International Science Center
Thousand Oaks, CA 91360†

ABSTRACT

Brittle materials are subject to microcrack formation at grain boundaries and at second phase particles. These cracks are induced by residual stress that results from incompatibilities in thermal contraction. The development of residual stress and its partial relaxation by diffusion (at elevated temperatures) are described. The evolution of microcracks within the residual stress fields are then examined. Particular attention is devoted to considerations of the critical microstructural dimension at the onset of microcracking.

INTRODUCTION

Many properties of ceramic materials depend on the incidence of microcracking. The most notable physical characteristics that exhibit a strong dependence on microcrack formation are certain mechanical (fracture toughness[1] and fracture strength[2]) and thermal (thermal diffusivity[3]) properties. The formation of stable microcracks is primarily related to localized residual stresses that develop because of thermal contraction mismatch or anisotropy (the

former in multiphase materials[4] and the latter in single phase materials[5]). Significant progress has recently been achieved in the analysis of microcracking events by using a combination of stress analysis (based on the Eshelby concept) and fracture mechanics.[5,6,7] The intent of this paper is to examine the microcracking phenomenon in order to emphasize both the progress that has been achieved and the limitations of the available analyses.

One of the dominant characteristics of microcracking is its dependence on the scale of the microstructure. Typically, there is a "critical" microstructural dimension, ℓ_c, below which microcracking is not generally observed and above which a significant density of microcracks becomes evident.[4,8,9] The development of a capability for predicting ℓ_c is a primary objective of microcracking analyses. A critical comparison with measured values of ℓ_c is also a demanding test of the validity of such analyses.

The amplitude of residual stress fields produced by thermal contraction mismatch is independent of the scale of the microstructure. A criterion for microfracture based on the peak tension would not, therefore, yield a size dependence. This dilemma was first addressed by suggesting[8] that the onset of microfracture be dictated by an equality of the loss of strain energy and the increase in surface energy associated with the microfracture event. The former is a volume dependent term, and the latter is a surface area term; hence, a critical size emerges in a natural way. A reasonable correspondence with experimental observation was achieved by specifying the ratio of the final crack size to the dominant dimension of the microstructure. A conceptual difficulty with the approach arises because only the thermodynamics of the initial and

final stages of the fracture event are considered; whereas, fracture is dictated by the rate of energy change at the critical condition for unstable crack extension.[5,9]

Subsequently, since size effects in brittle fracture often derive from statistical considerations,[10] a potential role of flaw statistics was suggested.[11] Notably, since fracture initiates from small inhomogeneities (pores, inclusions, etc.), the spatial and size distribution of these fracture initiating sites can influence the incidence of fracture. However, if the size distribution of these inhomogeneities is independent of the scale of the microstructure, the fracture probability for a constant volume fraction of the responsible microstructural phase would either be independent of size (volume distributed inhomogeneities)[12] or decrease with increase in size (interface distributed inhomogeneities).[13] A statistically based argument must, therefore, invoke inhomogeneities that increase in size as the microstructure enlarges. This effect is a plausible possibility, because inhomogeneities (such as pores) tend to increase in size during sintering, in direct proportion to the size of the grains[14] (or other microstructural entities). However, in the absence of well-substantiated distribution functions to describe the inhomogeneity size, the quantitative utility of the statistical approach is limited.

More recently, it has been recognized that a size effect can stem directly from considerations related either to the gradient of the residual stress field[5,6] or to stress relaxation.[7] For example, if the fracture initiating inhomogeneity is of sufficient size that it experiences an appreciable gradient of stress, then dimensional considerations demand that the fracture be size

dependent. Specifically, the stress intensity factor, K, is given by[5]

$$K \sim \sqrt{a} \int_0^1 \sigma(x/\ell)\, F(x/a)\, d(x/a) \tag{1}$$

where a is the inhomogeneity size, σ is the stress and F(x/a) is the appropriate Green's function. Since the stress can always be expressed in the form

$$\sigma(x/\ell) = \hat{\sigma}\, \Omega(x/a,\ a/\ell) \tag{2}$$

where $\hat{\sigma}$ is the peak residual tension, the stress intensity factor can be written

$$\frac{K}{\hat{\sigma}\sqrt{\ell}} = \sqrt{\frac{a}{\ell}} \int_0^1 \Omega(x/a,\ a/\ell)\, F(x/a)\, d(x/a) \equiv \kappa(a/\ell) \tag{3}$$

where $\kappa(a/\ell)$ is the function determined by integration. Now, if the stress intensity factor is equated to its critical value for crack extension, K_c, Eq. (3) yields a "critical size" given by

$$\ell_c = \left(\frac{K_c}{\hat{\sigma}\, \kappa(a/\ell)} \right)^2 \tag{4}$$

An additional size influence derives from the diffusive stress relaxation that can occur at elevated temperatures.[15] The rate of relaxation will be more rapid in fine-grained materials, because of the enhanced diffusive fluxes. Smaller residual stresses will thus obtain and the tendency for microcrack formation will be reduced.

The considerations of microcracking developed in this paper relate primarily to the size effect that derives from residual stress gradients and relaxation phenomena. Beyond the scope of this review are the residual stresses[6,17] produced by phase transformations during cooling (as in the ZrO_2 based alloys) and the effect of externally applied stress fields on the residual stresses and the onset of microcracking.

RESIDUAL STRESSES

Residual stresses typically encountered in ceramic materials derive from differences in thermal contraction (anisotropy of the thermal expansion coefficient, α, for a single phase material, and contraction mismatch for multiphase systems). Thermal contraction differences are important because ceramics are fabricated at elevated temperatures (by hot pressing or sintering) and, during cooling, stress relaxation (by diffusion or viscous flow) becomes sufficiently inoperative below a temperature T_g that appreciable local stresses must develop from the contraction mismatch. The elastic stresses that evolve below T_g can be computed by using adaptations of the Eshelby approach.[16]

Several such calculations will be presented below. A more difficult problem to address is the definition of T_g; this is also examined in the following section.

Elastic Stresses

The stresses that develop below T_g, calculated by using the Eshelby approach, are illustrated for the anisotropic contraction of a hexagonal grain in Fig. 1. This method of calculation first extracts the microstructural entity (or entities) subject to shape deformation and its shape is then allowed to change (as characterized by the unconstrained transformation strain ε^T_{ij}). Subsequently, its shape is restored to the shape of the matrix cavity (by exerting a uniform stress) and it is then reinserted into the cavity. Finally, interface forces are applied (of equal magnitude, but opposite sign, to the restoring stress) to achieve continuity of stress. For isolated particles of ellipsoidal geometry this process yields a uniform stress within the particle; hence, stress analysis is relatively straightforward. More complex behavior is expected for other geometries, such as individual grains within a polycrystalline aggregate.

Multiphase Materials

The stresses within a spherical particle subject to transformation strains ε^T (hydrostatic) and $'\varepsilon^T_{ij}$ (deviatoric) are[16,17]

$$\sigma^I = - \frac{\varepsilon^T}{(1 + \nu_m)/2E_m + (1 - 2\nu_p)/E_p} \tag{5a}$$

$$'\sigma^I_{ij} = - \frac{'\varepsilon^T_{ij}}{(1 + \nu_p)/E_p + 2(1 + \nu_m)(4 - 5\nu_m)/E_m(7 - 5\nu_m)} \tag{5b}$$

where σ^I is the hydrostatic stress and $'\sigma^I_{ij}$ is the deviatoric stress. The same hydrostatic stress level pertains for ellipsoidal particles, irrespective of their shape; but, the deviatoric stress is sensitive to the particle shape.[16] Two extremes are of interest. First, if the particles and matrix have isotropic thermal contraction coefficients, the resultant stress is exclusively hydrostatic; hence,

$$\sigma^I = - \frac{(\alpha_m - \alpha_p)\ (T_g - T)}{(1 + \nu_m)/2E_m + (1 - 2\nu_p)/E_p} \tag{6}$$

where $\alpha_m - \alpha_p$ is the thermal contraction mismatch between matrix and particle, and T is the temperature. For a particle and matrix with similar elastic constants, Eq. (6) becomes

$$\sigma^I = - \frac{(\alpha_m - \alpha_p)\ (T_g - T)\ E}{3(1 - \nu)} \tag{7}$$

Second, if the particle exhibits anisotropy of thermal expansion (e.g., α_1 and α_2), such that the average expansion matches that of the matrix, then the stress within the particle is purely deviatoric and is given by

$$'\sigma^I_{ij} = - \frac{(\alpha_m - \alpha_2)\ (T_g - T)}{(1 + \nu_p)/E_p + 2(1 + \nu_m)(4 - 5\nu_m)/E_m(7 - 5\nu_m)} \tag{8}$$

which for uniform elastic properties reduces to

$$\sigma_{ij}^{I} = - \frac{(7 - 5\nu)(\alpha_m - \alpha_2)(T_g - T)\, E}{15(1 - \nu^2)} \tag{9}$$

In general, therefore, the resultant stress, σ_{ij}, for uniform elastic constants is

$$\frac{\sigma_{ij}}{E(T_g - T)} = - \frac{(7 - 5\nu)(\alpha_m - \alpha_2)}{15(1 - \nu^2)} - \frac{(\alpha_m - \alpha_p)}{9(1 - \nu)}\, \delta_{ij} \tag{10}$$

The equivalent result for ellipsoidal geometry is

$$\frac{\sigma_{ij}}{E(T_g - T)} = - \frac{(\alpha_m - \alpha_p)}{9(1 - \nu)}\, \delta_{ij} - \frac{\gamma}{(1 + \nu)} (\alpha_m - \alpha_2) \tag{11}$$

where γ is a function of the particle shape.[16] For a needle, $\gamma = 1/2$; for a sphere, $\gamma = (7 - 5\nu)/15(1 - \nu)$; and for a disc, $\gamma = \pi(c/b)\,(2 - \nu)/4(1 - \nu)$, where c is the disc thickness and b is the disc radius.

The stresses within the matrix are more difficult to analyze and, with the exception of spherical[18] and cylindrical particles,[19-21] have not been computed exactly. Eshelby shows that if the harmonic and biharmonic potentials of the particle (however arbitrary its shape) are known, then the displacements in the matrix are related to the transformation strain ϵ_{ij}^{T} in the particle by

$$u_i = \frac{\sigma_{jk}^{T}\, \Psi_{,ijk}}{16\pi\mu(1 - \nu)} - \frac{\sigma_{ik}^{T}\, \sigma_{,jk}}{4\pi\mu} \tag{12}$$

where σ^T_{jk} is the stress derived by Hooke's law from the strain ε^T_{ij}. The matrix stresses can then be obtained from the displacement derivatives. In the case of a spherical particle subject to hydrostatic strain, the matrix stresses are particularly simple,

$$\sigma_{rr} = \sigma(r_o/r)^3, \qquad \sigma_{\theta\theta} = -(\sigma/2)(r_o/r)^3 \tag{13}$$

where r_o is the particle radius and r is the distance from the particle center.

The harmonic and biharmonic potentials for a very long cylindrical particle (fiber) have recently been calculated[20] and may be used to compute the matrix stresses from Eq. (12):

$$\phi = 2\pi r_o^2 \, \ell n \, (r/r_o) \tag{14a}$$

$$\psi = \pi r_o^2 (r^2 - r_o^2) - \pi r_o^2 \, r^2 + r_o^2/2 \, \ell n \, (r/r_o) \tag{14b}$$

For the case of thermal contraction mismatch between the fiber and matrix, described by a hydrostatic strain ε^T, the matrix stresses are

$$\sigma^c_{11} = E \, \varepsilon^T \frac{(3 - 2\nu)}{2(1 - \nu)} \frac{r_o^2(x^2 - y^2)}{r^4}$$

$$\sigma^c_{22} = -\sigma^c_{11} \tag{15}$$

$$\sigma^c_{12} = E \, \varepsilon^T \frac{(3 - 2\nu)}{2(1 - \nu)} \frac{r_o^2 \, xy}{r^4}$$

A case of particular interest is that of the cylindrical particle exhibiting an anisotropy of thermal contraction in the plane perpendicular to the long axis of the cylinder such that the average contraction matches that of the matrix. The stresses generated within the matrix are of the form[21]

$$\sigma_{11}^{c} = \frac{E\,\varepsilon_{11}^{T}}{(1+\nu)(1-2\nu)}\left[\frac{r_o^2\,(x^2-y^2)}{r^4} + \frac{\nu}{1-\nu}\,\frac{(x^4-y^4)}{r^2}\right]$$

$$+ \frac{E\,\varepsilon_{11}^{T}}{4(1-\nu^2)}\left[\frac{4r_o^2\,y^2(3x^2-y^2)}{r^6} + \frac{3r_o^2\,(x^4+y^4-6x^2y^2)}{r^2}\right] \qquad (16)$$

where

$$\varepsilon_{11}^{T} = (\alpha_1 - \alpha_m)(T_g - T)$$

However, since the stresses immediately adjacent to the interface are of greatest interest for microfracture problems, some pertinent information can be obtained by deriving the stresses in the matrix just outside the inclusion. For an ellipsoidal inclusion subject to dilatation, the stresses in the matrix can be written quite generally as:[16]

$$\sigma_{ij}^{I} = \sigma^{I}(n_i n_j - 1/3\delta_{ij}) \qquad (17)$$

where n_{ij} are the normals to the ellipsoid surface. Particular values for the stresses at the particle matrix interface have been calculated for disc and needle shaped particles.[22] The stresses are a maximum near the termination of the major axis of the ellipsoid. However, as described earlier, the gradient in stress (in addition to the stress level at the particle interface) is of importance in dictating the size effect. As far as the authors are aware, the stress gradients around ellipsoidal particles subject to a transformation strain have not been calculated and remain a subject for further work.

Single Phase Materials

Grains in single phase materials exhibit relatively complex geometric configurations, and stress analysis is more complex than for the isolated ellipsoidal particle. However, some useful approximations can be obtained quite straightforwardly. The general level of residual stress within the grains can be obtained by simply requiring a grain to be contained within an isotropic ma-

trix, with the average properties of the polycrystalline aggregate, and inserting the anisotropic contraction coefficients into Eq. (10). However, this simplification neglects the stress enhancing influence of grain junctions, an effect which has important consequences for microfracture.

Estimates of the stresses that develop in the vicinity of grain junctions can be obtained by adopting two-dimensional analogues, such as an array of hexagonal grains. The stresses that develop in such an array can be determined by firstly establishing the resultant body forces at each grain boundary facet (see Fig. 1). These body forces, p, generate non-uniform stresses that superimpose upon the uniform stresses developed during shape restoration. Of principal interest are the stresses at the grain boundaries, because these are the dominant sites for microfracture. The stresses at a site (x,z) inclined at an angle β to the boundary, (Fig. 2) are of the form[5]

$$\frac{4\pi\sigma_{xx}}{p\cos\beta} = \int_0^1 \frac{(z + \alpha\sin\beta)}{[\alpha^2 - 2\alpha(z\sin\beta - x\cos\beta) + (x^2 + z^2)]}$$

$$\left\{(1 - \nu) - \frac{2(1 + \nu)(\alpha\cos\beta - x)^2}{[\alpha^2 + 2\alpha(z\sin\beta - x\cos\beta) + (x^2 + z^2)]}\right\} d\alpha \qquad (18)$$

Equation (18) should be used to obtain the stresses on boundary AB (Fig. 3) from the body forces of the four adjacent boundaries (AA', AA", BB', BB"). For more remote boundaries sufficient accuracy can be achieved by placing a single force at the grain facet center,[23] which represents the total body force on that boundary (Fig. 3). These stresses superimpose on a uniform stress (equal in magnitude to half the initial stress) which derives from the body forces on AB coupled with the initial stress.

The component of the stress from the four adjacent boundaries dominates the behavior in the vicinity of the grain junction. This stress component is of the form[5]

$$\frac{4\pi\sigma}{p \cos \beta} = A_1(\beta,\nu)\ \ell n \left[\frac{\ell^2 + x^2 + z^2 + 2\ell(z \sin \beta - x \cos \beta)}{x^2 + z^2}\right]$$
$$+ A_2(\beta,\nu,x,z) \cdot \tan^{-1}\left[\frac{2\ell + z \sin \beta - x \cos \beta}{2(z \cos \beta + x \sin \beta)}\right]$$
$$- \tan^{-1}\left[\frac{z \tan \beta - x}{2(z + x \tan \beta)}\right] + A_3(\ell, \beta, \nu, x, z) \qquad (19)$$

where A_1, A_2, and A_3 are relatively complex functions in the range $\pm 2\pi$. The logarithmic term is singular at the grain junction and is thus the most influencial with regard to microcrack formation.[5]

The specific stress magnitudes that develop depend on the relative orientations of the grains circumventing the boundary of interest. Preliminary calculations have been conducted for the orientation that has been assumed to yield the maximum stress; this depicted in Fig. 4a, and the results are shown in Fig. 4b. Calculations for more general grain orientation relations are now in progress.[23] These results will provide a full perspective of residual stress distributions in polycrystalline aggregates in which there is a random distribution of contraction anisotropy orientations.

STRESS RELAXATION EFFECTS

Stress relaxation in ceramics occurs primarily by diffusion (or by viscous flow in the presence of an amorphous phase). These relaxation processes are usually motivated by local gradients in hydrostatic stress, and thus occur in response to localized thermal contraction stresses, while the material is at elevated temperatures.

Multiphase Materials

For isotropic multiphase materials, there is no gradient of hydrostatic stress within the isolated phase (Eq. 5). However, large shear stresses exist within the surrounding matrix (note that the hydrostatic stress is zero). The shear stresses within the matrix cause grain boundary sliding, and diffusive deformation will occur in response to local normal stresses induced by

sliding.[24] The deformation field will be similar to that of a cavity subject to internal pressure. Initially, radial flow in the matrix will redistribute the residual stress. Reduction of the stresses will begin when the redistribution extends across the sample, following the onset of interaction between the stress fields around adjacent particles. The authors are not aware of solutions for this problem, although the analysis is relatively straightforward.

Polycrystalline Single Phase Aggregates

It has already been demonstrated that anisotropic thermal contraction in polycrystalline aggregates develops tensile or compressive stresses on grain boundaries. A gradient of chemical potential suitable for diffusive relaxation (Fig. 5) is thus established. The "initial" stress involves singularities near grain junctions (Fig. 4). But the singularities are weak (logarithmic) and should be rapidly dispersed by localized diffusive fluxes. The rate controlling relaxation process involves diffusion between adjacent grain facets (Fig. 5), such that atoms are removed from the boundaries subject to compression and are deposited on boundaries under tension. If it is assumed that the relaxation times are sufficiently rapid that atom deposition and removal occurs uniformly along the respective grain boundaries, a parabolic "steady-state" stress distribution must develop along the boundaries during the relaxation process. The extent of strain relaxation can then be deduced by using well-established mathematical procedures for diffusive flow. This mode of analysis is only permissable when the diffusivities are large, notably at the highest temperatures. The stress evolution at intermediate temperatures requires "transient" solutions involving more complex formulations. Such analyses have not yet been performed. Currently, therefore, it is only possible to obtain approximate solutions by permitting "steady-state" relaxation above a "freezing" temperature T_s and invoking fully elastic stress development below T_g.

The stress relaxation problem can be posed by first establishing the normal elastic displacement δ_1 of the boundaries during cooling (the driving force for the diffusive flow, Fig. 5) and the displacement relaxation δ_2 due to diffusion.

Then, the resultant displacement δ (= δ_1 - δ_2), which determines the level of the relaxed stress, can be derived. The solution for a constant cooling rate $\dot{T}$ will be presented.[25]

The elastic stress level on a grain boundary normal to the direction of maximum contraction is

$$\sigma_{xx} = \frac{\beta E(T_o - \dot{T}t)\Delta\alpha}{(1 + \nu)} \tag{20}$$

where T_o is the initial temperature, $\Delta\alpha$ is the deviation of the contraction coefficient from the average, and β is a coefficient that depends on the orientations of the adjacent grains. The corresponding elastic displacement is

$$\delta_1 = \frac{\sqrt{3}\ \ell\ \beta\ \dot{T}\ t\ \Delta\alpha}{2\ (1 + \nu)} \tag{21}$$

The relaxations of these displacements by diffusion are governed by the relation[26]

$$\frac{d^2\sigma(x,t)}{dx^2} = -\frac{kT\dot{\delta}_2(t)}{\Omega\ D_b\delta_b} \tag{22}$$

where $D_b\delta_b$ is the diffusion parameter, Ω the atomic volume and $\dot{\delta}$ is assumed to be uniform (as noted above). Integration of Eq. (22) gives the stress distribution

$$\sigma(x,t) = \frac{-\xi x^2}{2} + C_1 x + C_2 \tag{23}$$

where $\xi = kT\dot{\delta}_2(t)/\Omega\ D_b\delta_b$ and C_1 and C_2 are the integration constants. The positions of zero flux ($d\sigma/dx = 0$) in the system are at the grain facet center O and at the grain junction J (Fig. 5). Hence, since the flux must be continuous at the grain corner A, the constant C_1 must be equal to $\xi\ell/2$. If σ_o is the stress at A, the stress distribution becomes

$$\sigma(x,t) = -\frac{\xi x^2}{2} + \frac{\xi x \ell}{2} + \sigma_o \tag{24}$$

The equivalent average stress is

$$\langle\sigma\rangle(t) = \frac{\xi \ell^2}{12} + \sigma_o \tag{25}$$

Volume conservation requires that the volume of material deposited on the tensile boundary must equal the volume removed from the compressed boundary. The stress at the grain corner thus becomes

$$\sigma_o = \xi \ell^2/12 \tag{26}$$

and the average stress reduces to

$$\langle\sigma\rangle(t) = \frac{kT\ell^2 \dot{\delta}_2}{6\Omega D_b \delta_b} \tag{27}$$

The average stress on each boundary must also be related to the resultant displacement of the grain:

$$\frac{\sqrt{3}\ell}{2E} \frac{d\langle\sigma\rangle}{dt} = \dot{\delta}_1 - \dot{\delta}_2 \tag{28}$$

Substituting $\dot{\delta}_1$ from Eq. (21) and $\dot{\delta}_2$ from Eq. (27), and noting that D_b is temperature dependent

$$D_b = D_o e^{-Q/kT} \tag{29}$$

where Q is the activation energy for boundary diffusion, the following differential equation obtains

$$\frac{d\langle\sigma\rangle}{dT} - \frac{12\Omega\delta_b D_o E}{\sqrt{3}k\ell^3 \dot{T}} \frac{e^{-Q/kT}}{T} \langle\sigma\rangle = - \frac{\beta E \Delta\alpha}{(1 + \nu)} \tag{30}$$

The solution to this equation must be conducted numerically. However, an approximate series expansion may be derived[25] for comparison with the elastic result expressed in terms of a "freezing" temperature T_g:

$$\frac{\langle\sigma\rangle(1+\nu)}{\beta E \Delta\alpha} = T_g - T$$

From this, T_g is given approximately by

$$T_g \sim \frac{Q/k}{\ell n[12\Omega D_o \delta_b E/\sqrt{3}nk\ell^3 \dot{T}]} \tag{31}$$

The trends in T_g with the influential variables are immediately apparent. In particular, T_g increases as the grain size and cooling rate increase and as the diffusivity and modulus decrease. This behavior is exemplified for Al_2O_3 ($D_o\delta_b = 10^{-9}$ m^3 s^{-1}, Q = 100 kcal/mole, $\Omega \sim 10^{-29}$ m^3, n = 30, E = 420 GN m^2), for which:

$$T_g = \frac{50{,}000}{29.5 - \ell n\, \ell^3 \dot{T}}$$

where ℓ is in microns, T in K s^{-1} and T_g is in K. Specifically, for ℓ = 1 μm and T = 1K s^{-1}, T_g = 1695K; whereas for ℓ = 10 μm and T = 1K s^{-1}, T_g = 2210K.

MICROCRACK FORMATION

The formation of microcracks at grain boundaries or at second phase particles has been considered to depend on the existence of a distribution of small inhomogeneities that pre-exist at the boundaries (especially at three grain junctions) or interfaces.[5,6,7] These inhomogeneities have been proposed because the stress intensification levels associated with the residual stress fields do not appear to be of sufficient magnitude to induce fracture in defect free material (although further study is needed to establish whether this possibility can be discounted). The role of the proposed inhomogeneities is to further enhance the stress intensification to a level suitable for microcrack evolution. It is certainly reasonable to presume that inhomogeneities do exist at boundaries or interfaces in ceramics, e.g., small pores remaining at grain triple points. However, little effort has yet been devoted to the elucidation of the inhomogeneities that induce microfracture in specific miocrostructural

situations. It is thus generally assumed that the inhomogeneities exhibit the stress concentrating properties of small microcracks: a presumption that is evidently an over-simplification. Thereafter, stress intensity factors can be calculated (from the residual stress levels) and compared with the critical values for grain boundary separation. Approximate stress intensity factors are conveniently calculated with a superposition method, based on the prior stress field.[5,6] A typical example, illustrated in Fig. 6, is where a microcrack develops along two symmetrically stressed grain facets, initiating at the common triple junction. The stress intensity factor for such a crack is given by

$$\frac{K(1+\nu)}{E\Delta\alpha\Delta T\sqrt{\ell}} = \kappa(a/\ell) \tag{32}$$

where $\kappa(a/\ell)$ is the function plotted in Fig. 6. It is noted that the stress intensity factor exhibits a maximum, $\hat{K}$. This is typical of crack extension in residual or spatially varying stress fields. The principal maximum in the present analysis essentially coincides with a crack front located at the first triple junction, where the residual stress changes sign (i.e., the residual stress becomes compressive along the impinging boundaries). Equating K to the boundary separation resistance, K_c^b, yields an <u>absolute minimum</u> condition for the formation of microcracks. This corresponds to an <u>upper bound</u> for the critical grain facet size;

$$\hat{\ell}_c = \left[\frac{K_c^b\,(1+\nu)}{\hat{\kappa}\,E\Delta\alpha\Delta T}\right]^2 \tag{33}$$

where $\hat{\kappa}$ is the magnitude of the normalized stress intensity factor at the maximum. Estimates of specific values of the grain facet sizes that induce microcracking involve statistical considerations based on flaw distributions.

More exact calculations of the stress intensity factor can be obtained by using numerical (finite element or finite difference) methods. A recent example[7] is the use of a finite difference scheme for calculating the stress

intensity factor for a crack at the interface of a spherical second phase particle. A convenient use of the finite difference method involves the calculation of the strain energy, U, as a function of crack length, a. The stress intensity factor is then deduced from the crack length derivative of the strain energy. A maximum value, $\hat{K}$, is obtained. The corresponding absolute minimum requirement for microcrack initiation is

$$\hat{R}_c = \frac{1.2(K_c^I/\langle\sigma\rangle)^2}{(1 - \nu)} \tag{34}$$

where K_c^I is the resistance of the interface to fracture and $\langle\sigma\rangle$ is the stress in the uncracked particle.

Further progress in the elucidation of microfracture is achieved by incorporating defects that reduce the critical size below the upper bound values. Little progress has yet been achieved in selecting appropriate defects and defect size distributions; although results could clearly be obtained by selecting arbitrary distributions (such as one of the extreme value distributions). Careful obsevations coupled with pertinent stress intensity factor calculations are needed to establish a more fundamental appreciation of microcracking. Comparison of the available calculations of K with experimental observations of microcracking suggest[5,6,7] that triple point defects in the size range, $0.1 < 2a/\ell < 0.3$, are typically involved in the microcrack initiation process. However, more direct observations and further calculations are needed to substantiate and refine this result.

CONCLUSION

This paper has described methods for calculating the residual stresses that develop at the microstructural level because of thermal contraction inhomogeneity. The stresses are typified by locally large amplitudes (with some singularities) and rapid gradients. These characteristics are central to the onset of microcracking, both microcrack initiation and arrest.

The stress level is also shown to depend on the rate of stress relaxation

at elevated temperatures, by diffusion or viscous flow. The relaxation rate is a strong function of microstructure: rapid relaxation rates obtain in fine grained materials or in materials containing an amorphous boundary phase. These relaxation effects have been demonstrated to be manifest in an effective freezing temperature, a temperature at which elastic residual stresses begin to develop.

The onset of microcracking within the residual stress field has been considered to depend on the presence of small microstructural inhomogeneities (such as voids) at the susceptible interfaces. These features certainly exist, but have not yet been uniquely correlated with the onset of microcracking. By treating these pre-existent inhomogeneities as crack-like entities, stress intensity factors have been calculated. The level and variation in stress intensity factors indicate the potential for microcrack initiation and arrest at grain boundaries and interfaces.

In particular, a lower bound for the critical microstructural size needed to initiate microcracks has been identified (no microcracks can be observed at size levels below this bound). The actual formation of microcracks above the lower bound depends on the statistical characteristics (size and spatial) of the pre-existent inhomogeneities. This issue has not been addressed.

ACKNOWLEDGEMENT

The authors wish to thank the Office of Naval Research under Contract N-0014-79-C-0159. (AGE) and the Rockwell International Independent Research and Development Program (DRC) for their financial support, and the U.S. Department of Energy under Contract W-7405-ENG-48.

REFERENCES

1. R.G. Hoagland, G.T. Hahn and A.R. Rosenfield, Rock Mechanics 5, 77 (1973).

2. F.A. McClintock and H.J. Mayson, ASME Applied Mechanics Conf. (June 1976).

3. H.J. Siebenbeck, D.P.H. Hasselman, J.J. Cleveland and R.C.Bradt, Jnl. Amer. Ceram. Soc. 59, 241 (1976).

4. F.F. Lange, Fracture Mechanics of Ceramics (Ed. R.C. Bradt, D.P.H. Hasselman and F.F. Lange) Plenum, N.Y. Vol. 4 (1977).

5. A.G. Evans, Acta Met. 26, 1845 (1978).

6. D.R. Clarke, Acta Met., in Press.

7. Y.M. Ito, M. Rosenblatt, L.Y. Cheng, F.F. Lange and A.G. Evans, Int. J. Fract. (In Press).

8. R.W. Davidge and G. Tappin, Jnl. Mater. Sci 3, 297 (1968).

9. J.A. Kuszyk and R.C. Bradt, Jnl. Amer. Ceram. Soc. 56, 420 (1973).

10. W. Weibull, Ingenioers Vetenskaps Akad., 151, (1939).

11. A.G. Evans, Jnl. Mater. Sci., 9, 210 (1974).

12. O. Vardar, I. Finnie, D.S. Biswas and R.M. Fulrath, Intl. Jnl. Frac. 13, 215 (1977).

13. A.G. Evans, D.S. Biswas and R.M. Fulrath, Jnl. Amer. Ceram. Soc. 62, 95 (1979)

14. W.D. Kingery and B. Francois, in "Sintering and Related Phenomena," edited

G.C. Kuczynski, Gordon and Breach, 1967.

15. J.E. Blendell, R.L. Coble and R.J. Charles, in "Ceramic Microstructure '76," edited R.M. Fulrath and J.A. Pask, Westview Press, Boulder, 1977.

16. J.D. Eshelby, Proc. Roy. Soc., A241, 376 (1957).

17. A.G. Evans and A.H. Heuer, Jnl. Amer. Ceram. Soc. 63, (May/June 1980), to be published.

18. J. Selsing, Jnl. Amer. Ceram. Soc., 44, 419 (1961).

19. L.M. Brown and D.R. Clarke, Acta. Met. 25, 563 (1977).

20. D.R. Clarke, PhD Thesis, University of Cambridge (1974)

21. D.R. Clarke to be published.

22. G.C. Weatherly, Phil. Mag. 17, 791 (1968).

23. Y. Fu and A.G. Evans, to be published.

24. R. Raj and M.F. Ashby, Acta Met. 23, 653 (1975).

25. D.R. Clarke and A.G. Evans, to be published.

26. A.G. Evans and A.S. Rana, Acta Met., 28, 129 (1980).

27. R.M. Cannon and R.L. Coble, Deformation of Ceramics (Ed., R.E. Tressler and R.C. Bradt), Plenum, N.Y. (1975) p. 61.

FIGURE CAPTIONS

Fig. 1 A schematic indicating the Eshelby method for calculating the residual stresses and strains generated by anisotropic thermal expansion of an hexagonal grain.

Fig. 2 The linear boundary segment used to compute the relaxation stresses, showing the coordinate system (x, z).

Fig. 3 An hexagonal grain array showing the body forces used to calculate the stress at the central facet AB.

Fig. 4 The grain configuration that yields large values of the residual stress at facet AA' and the stresses calculated to exist along that facet.

Fig. 5 The elastic and diffusion displacement that occurs during cooling, indicating the direction of the diffusive flux. Also shown are the stresses that develop during steady-state diffusive flow.

Fig. 6 The variation of the normalized stress intensity factor with crack length for the grain, crack configuration indicated on the inset.

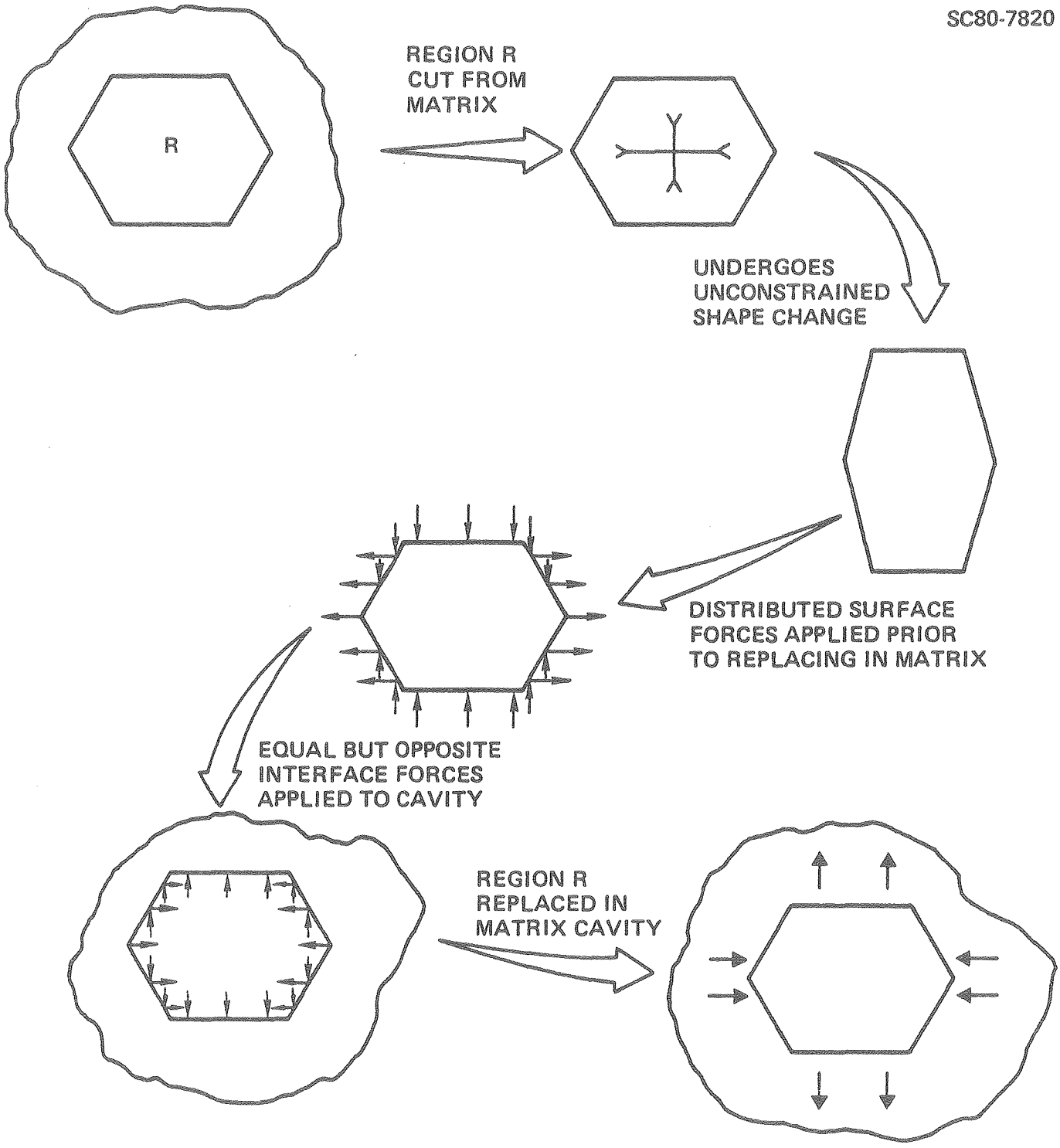
R
REGION R
CUT FROM
MATRIX
UNDERGOES
UNCONSTRAINED
SHAPE CHANGE
DISTRIBUTED SURFACE
FORCES APPLIED PRIOR
TO REPLACING IN MATRIX
EQUAL BUT OPPOSITE
INTERFACE FORCES
APPLIED TO CAVITY
REGION R
REPLACED IN
MATRIX CAVITY

Fig. 1

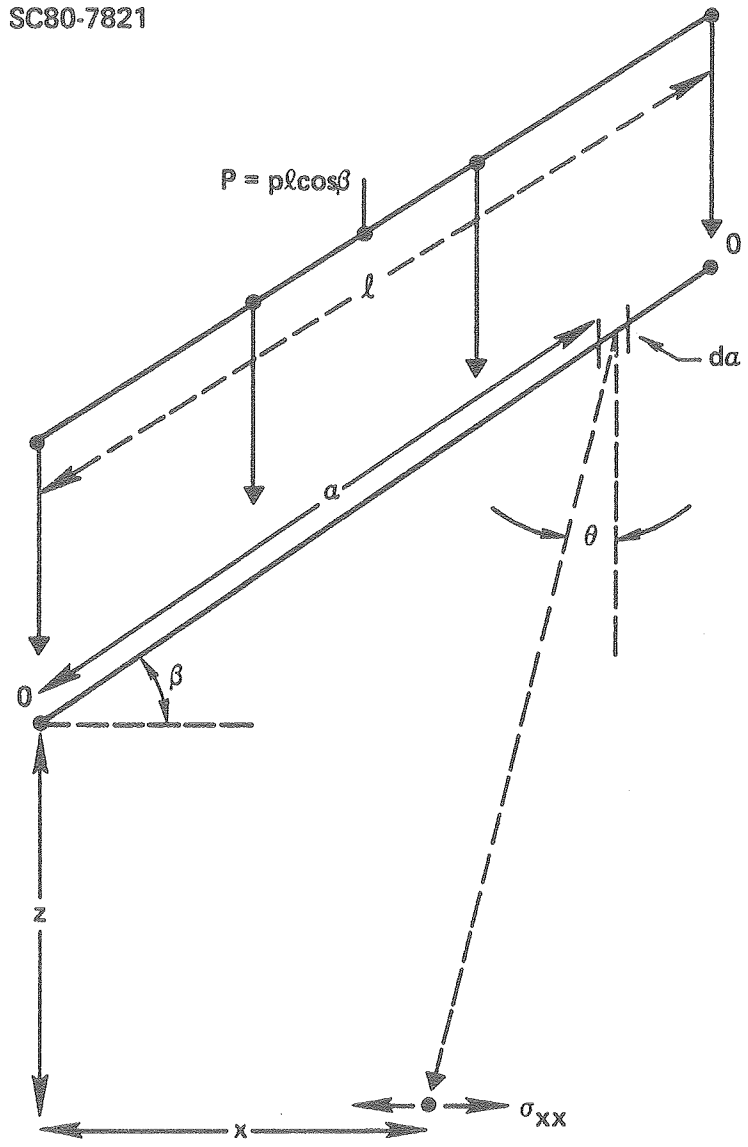

Fig. 2

SC80-7819

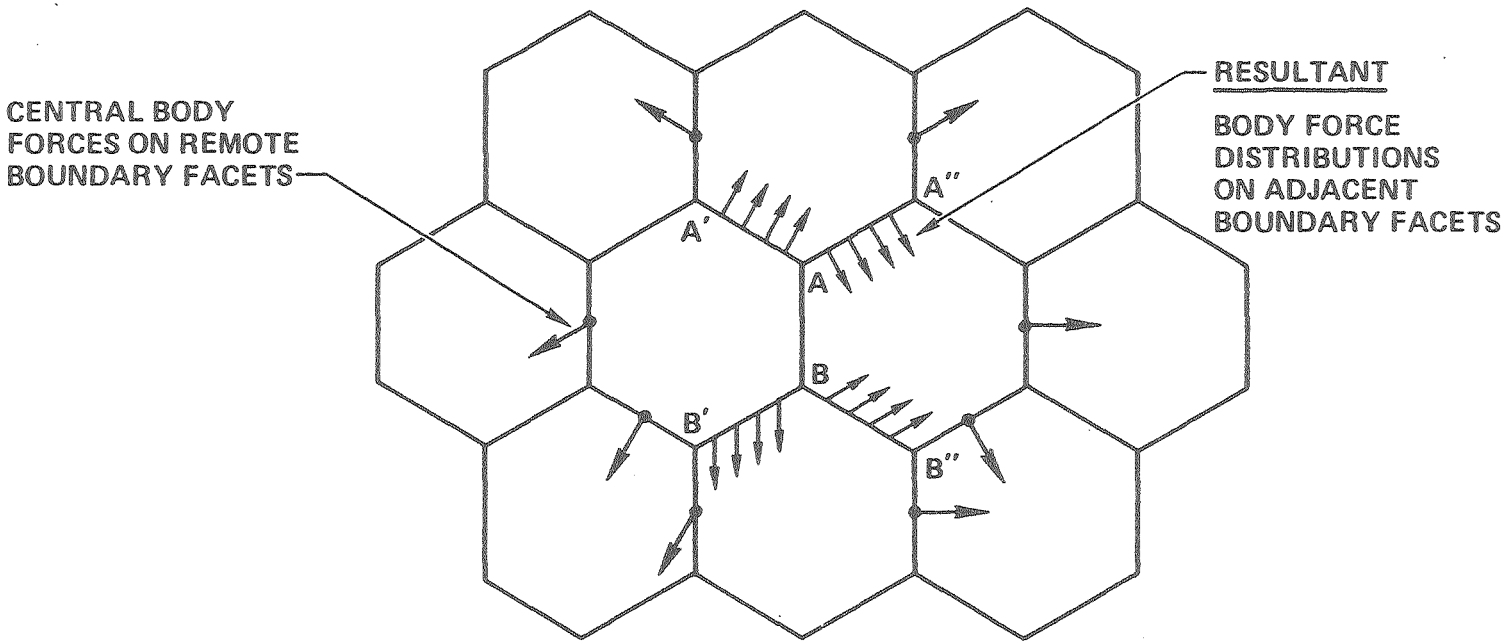

Fig. 3

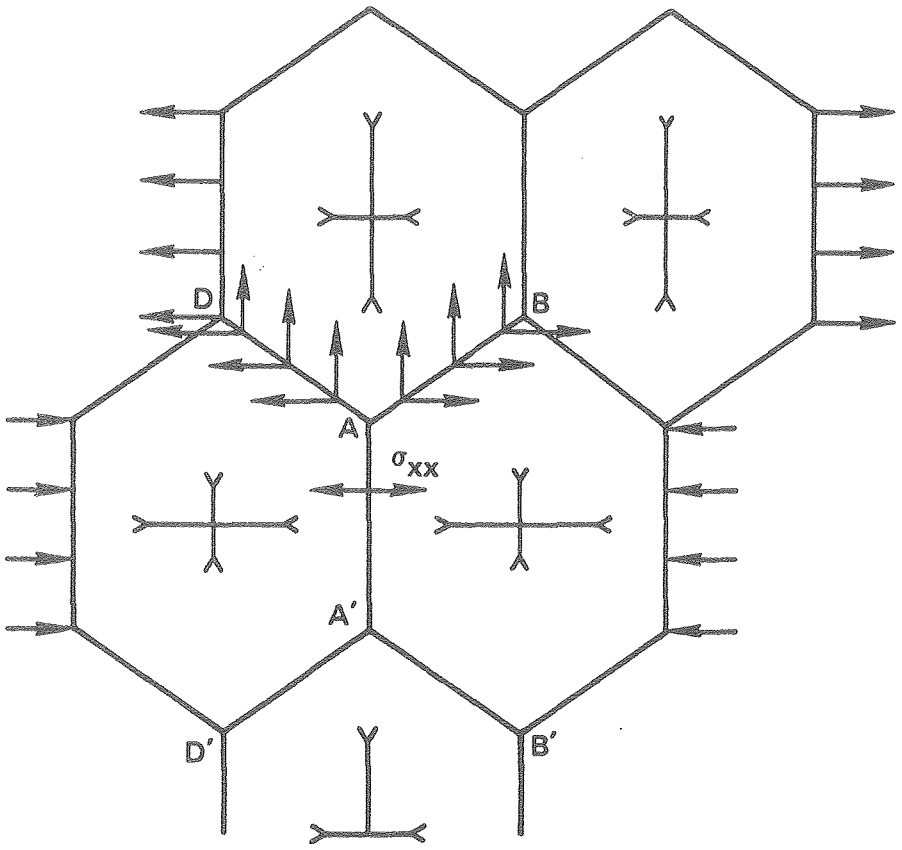
D
B
A
σ_{xx}
A'
D'
B'

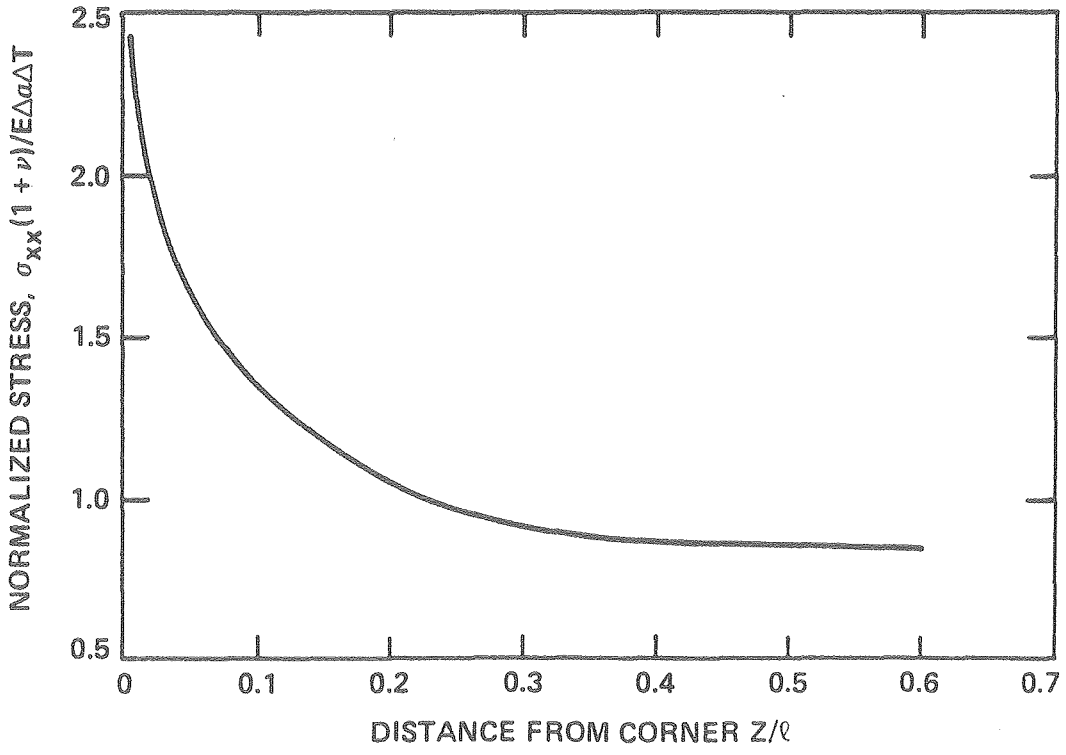
NORMALIZED STRESS, $\sigma_{xx}(1+\nu)/E\Delta a\Delta T$
2.5
2.0
1.5
1.0
0.5
0
0.1
0.2
0.3
0.4
0.5
0.6
0.7
DISTANCE FROM CORNER Z/ℓ

Fig. 4

SC80-7815

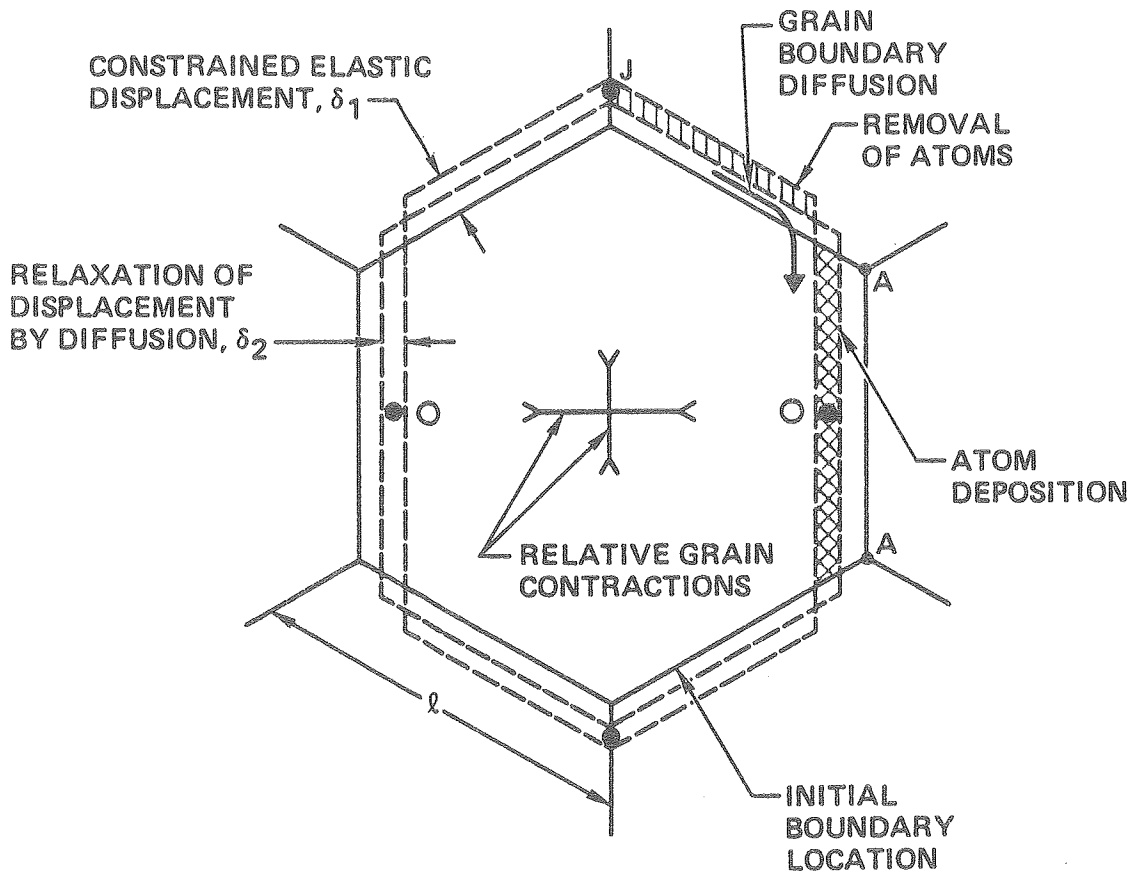

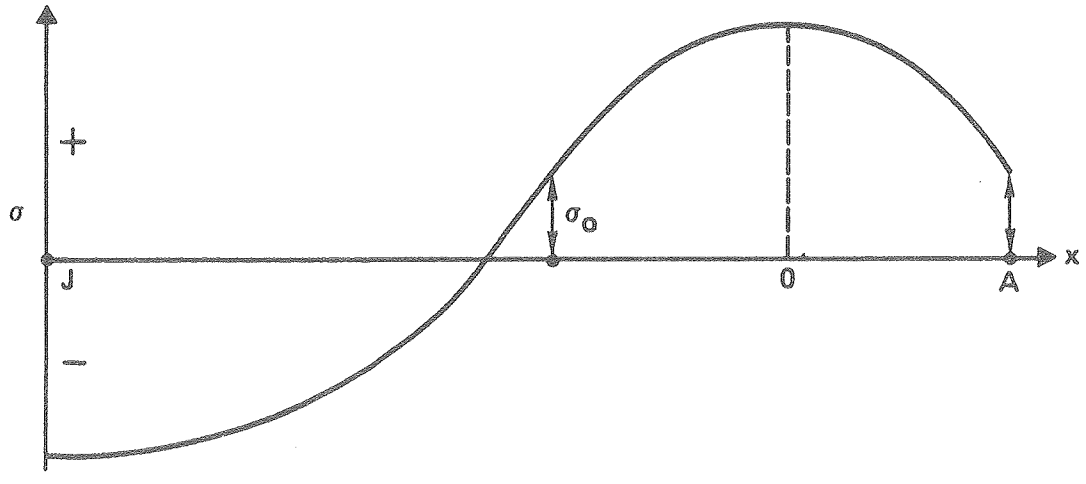

Fig. 5

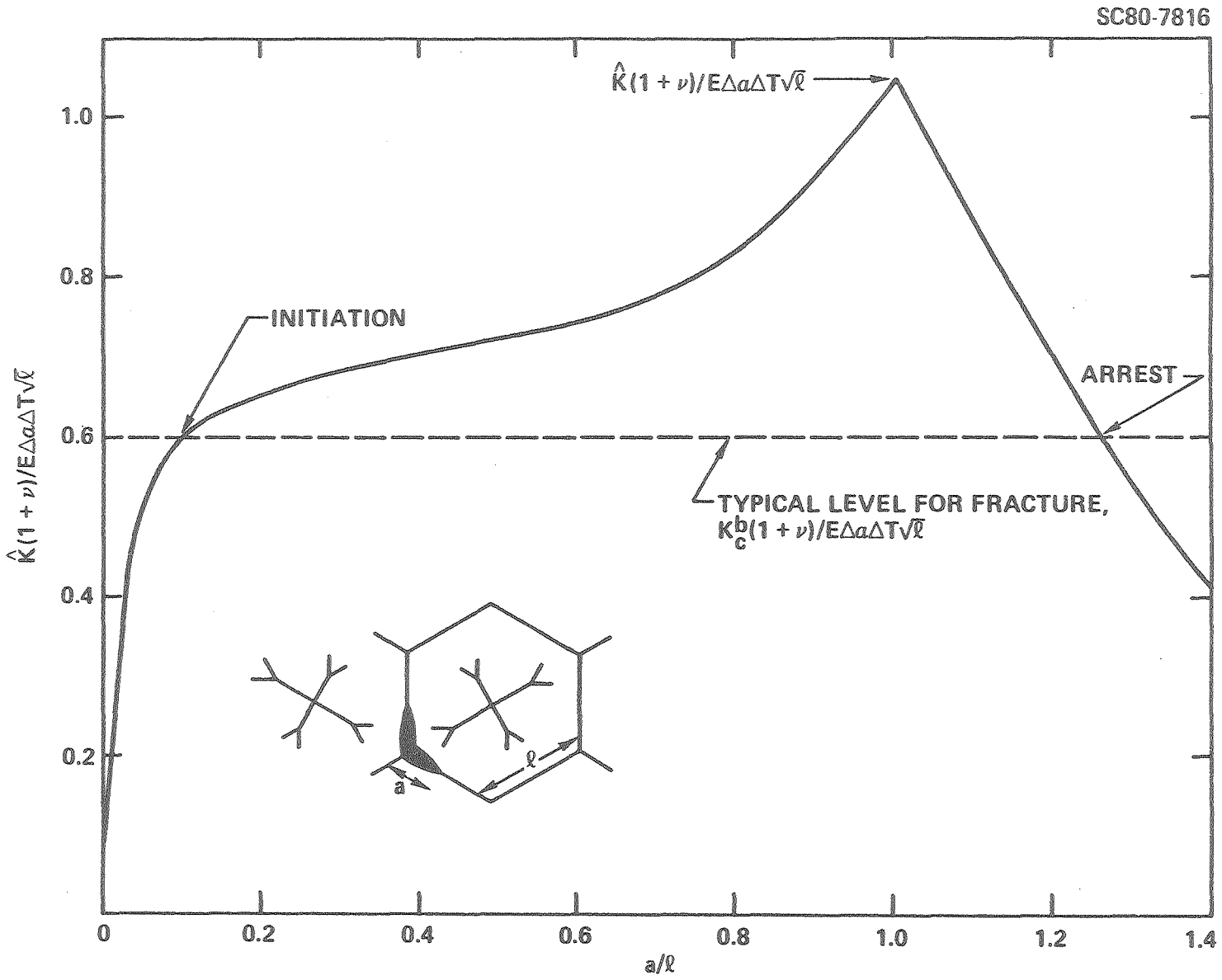
SC80-7816
$\hat{K}(1+\nu)/E\Delta a\Delta T\sqrt{\ell}$
INITIATION
ARREST
TYPICAL LEVEL FOR FRACTURE,
$K_c^b(1+\nu)/E\Delta a\Delta T\sqrt{\ell}$
a
ℓ
1.0
0.8
0.6
0.4
0.2
0
0.2
0.4
0.6
0.8
1.0
1.2
1.4
a/ℓ

Fig. 6